Sundararajan Natarajan*

On the application of the partition of unity method for nonlocal response of low-dimensional structures

Abstract: The main objectives of the paper are to (1) present an overview of nonlocal integral elasticity and Aifantis gradient elasticity theory and (2) discuss the application of partition of unity methods to study the response of low-dimensional structures. We present different choices of approximation functions for gradient elasticity, namely Lagrange intepolants, moving least-squares approximants and non-uniform rational B-splines. Next, we employ these approximation functions to study the response of nanobeams based on Euler-Bernoulli and Timoshenko theories as well as to study nanoplates based on first-order shear deformation theory. The response of nanobeams and nanoplates is studied using Eringen's nonlocal elasticity theory. The influence of the nonlocal parameter, the beam and the plate aspect ratio and the boundary conditions on the global response is numerically studied. The influence of a crack on the axial vibration and buckling characteristics of nanobeams is also numerically studied.

Keywords: axial vibration; Euler-Bernoulli beam; extended finite element method; flexural vibration; gradient elasticity; moving least-squares approximants; nonlocal integral elasticity; Timoshenko beam.

DOI 10.1515/jmbm-2014-0017

1 Introduction

The mechanical behavior of solids can be studied at three different length scales: (i) atomic/lattice scale, (ii) microstructure/grain scale and (iii) the continuum scale. The lattice theory takes into account a finite range of the interatomic forces, whereas the macroscopic (or local) theory of elasticity is based on the concept that the response forces of the body are contact forces, i.e., the forces have the zero range. Here, the material constants are estimated under bulk situation or similar continuum large scale and time scale. When there is an additional activity in the material (i.e., when small-scale effects become important, e.g., atomic cohesive force, surface and interface energy, non-equilibrium transport, defect formulation, etc.), then it is important to modify the continuum model with the help of atomic/lattice-scale and microstructure/grain-scale considerations.

In the atomic theory of lattices, the existence of long-range cohesive forces is well recognized and their effect on the dispersion of elastic waves is well documented [1]. The classical theory of elasticity being the long-wavelength limit of the atomic theory excludes these effects. The local theory can successfully describe a physical phenomenon by considering a very large number of molecules under equilibrium, but it fails when the physics is governed by the microstructure (dislocations and grain boundaries in crystals or network morphology in polymers and atomic cluster motion). The inherent assumption in local elasticity is that the dimensions of engineering structures are much larger than the characteristic dimensions of the microstructure. Thus, the classical continuum theories lack the capability of representing the size effects since they do not include any internal length scale [2]. Consequently, these theories fail when the specimen size or the wavelength becomes comparable with the internal length scales of the material.

In order to improve the local theory of elasticity, several modifications of the classical elasticity formulation have been proposed, such as the strain gradient theory [3], modified couple stress theory [4–9] and nonlocal elasticity theory [10–12]. A common feature of these theories is that they include one or several intrinsic length scales. The predictions of these theories reduce to those of local continuum theories when the specimen size is much larger than the internal length scale. The key idea of the nonlocal elastic approaches is that within a nonlocal elastic medium, the particles influence one another not simply by contact forces and heat diffusion but also by long-range cohesive forces. In this way, the internal length scale can be considered in the constitutive equations

***Corresponding author: Sundararajan Natarajan,** Department of Mechanical Engineering, Indian Institute of Technology-Madras, Chennai 600036, India, e-mail: snatarajan@cardiffalumni.org.uk; snatarajan@iitm.ac.in

simply as a material parameter as gradient coefficient or commonly known as the nonlocal parameter. One approach to estimate these nonlocal material parameters is by matching the phonon dispersion relation computed by these theories with the lattice dynamics dispersion relation [13–15].

Sun and Zhang [16] investigated the in-plane Young's modulus and in-plane and out-of-plane Poisson's ratio for ultra-thin films. Their result showed that the values of Young's modulus and Poisson's ratio depend on the number of atomic layers considered in the thickness direction and they approach the respective bulk properties as the number of atomic layers increases. Thus, the local continuum theories cannot be readily applied to study small-scale effects, since at small sizes the material microstructure, such as the lattice spacing between the individual atoms, cannot be neglected and, moreover, the discrete structure of the material can no longer be homogenized as done in local continuum theories. It is seen from the recent literature that the amount of work carried out on the application of nonlocal and/or gradient elasticity theories to study the response of nanobeams and nanostructures is considerably increasing. The following subsection outlines some of most recent contributions.

1.1 Background

1.1.1 Vibration of nanostructures

Eringen's nonlocal elasticity theory has been applied by several authors to study axial vibrations and free transverse vibrations of nanostructures [17–19]. Recently, the nonlocal beam models have been applied to investigate the static and vibration properties of single- and multi-walled carbon nanotubes (CNTs) [20–24]. As the small-scale effects have to be accounted for and the nonlocal theory seamlessly connects atomic lattice theory and continuum theory, via nonlocal moduli, there has been an increasing use of nonlocal elasticity theory to study the stability characteristics of CNTs [25–28]. It is also evident from the explicit solutions derived by Wang and Liew [21] for static deformation of micro- and nanostructures that the small-scale effects cannot be neglected. Duan et al. [29] derived exact solutions for axisymmetric bending of circular plates based on nonlocal plate theory. Duan et al. [30] calibrated the small scaling parameter e_0 for the nonlocal Timoshenko beam theory from molecular dynamics. Their results showed that the calibrated values of e_0 are different from published results. The parameter is a function of the length-to-diameter ratio, mode shapes and boundary conditions associated with single-walled CNTs (SWCNTs). Lu et al. [31] studied the dynamic characteristics of beams using the nonlocal elasticity model.

Reddy and Pang [32] derived the governing equations of motion for Euler-Bernoulli beams and Timoshenko beams using the nonlocal differential equations of Eringen [10] and presented closed-form solutions for beam static bending, vibration and buckling response with various boundary conditions. Recently, Reddy [33], based on von Karman nonlinear strains and Eringen's nonlocal theory, derived governing equations of equilibrium for beams. Phadikar and Pradhan [19] developed a variational formulation for Euler-Bernoulli beams and Kirchoff plates employing Hermite and Lagrange polynomials to study the response of beams and plates within the nonlocal elasticity framework. Roque et al. [34] studied bending, buckling and vibration of Timonshenko nanobeams using collocation techniques. Civalek and Demir [35] applied nonlocal Euler-Bernoulli beam theory to study static bending and vibration of microtubules using the differential quadrature method (DQM). The nonlocal linear elasticity theory of Eringen has been applied to study free in-plane vibration and flexural vibration of plates [36–38]. Reddy [33] and Aghababaei and Reddy [39] extended the classical, first- and third-order shear deformation theory using the nonlocal linear theory of elasticity and presented analytical solutions of bending and vibration of plates. The free vibration of single-layered and multi-layered graphene sheets has been studied using the first-order shear deformation nonlocal plate theory [37, 40].

1.1.2 Buckling of nanostructures

Wang et al. [25] based on the differential version of Eringen's nonlocal elastic model showed that the buckling solutions for CNTs via local continuum mechanics overestimate the response and the scale effect is indispensable. Murmu and Pradhan [41, 42] for the first time studied the buckling of SWCNTs embedded in an elastic medium using nonlocal elasticity and Timoshenko beam theory. Both Wrinkler-type and Pasternak-type models are employed to simulate the interaction of nanotubes with the surrounding elastic medium. The critical buckling loads are numerically obtained by using a DQM. Their study suggested that the buckling loads of SWCNTs strongly depend on the small-scale coefficients and on the stiffness of the surrounding medium. Pradhan [43] studied the buckling of nanoplates such as graphene sheets using a modified higher order shear deformation theory employing the nonlocal differential constitutive relations of Eringen. Zhang

et al. [27] proposed a nonlocal Donnell multi-shell model for the axial buckling of multi-walled carbon nanotubes (MWCNTs) with hinge ends under axial compression. Their results showed that the buckling modes and length of the tubes influence the small-scale effects on the axial buckling strain. By including both van der Waals forces and the effects of small length scales, Sudak [28] studied the buckling characteristics of MWCNTs. In a recent work, Pradhan and Murmu [44] have studied the buckling characteristics of a single-layer graphene sheet under biaxial compression. Their results showed that biaxially compressed graphene sheets showed a lower influence of nonlocal effects for the case of smaller side lengths and large nonlocal parameter values.

1.2 Objective

As seen earlier, the study of the response of low-dimensional structures relied on analytical approaches or numerical techniques. To the best of the author's knowledge, the existing numerical approaches are limited to using the DQM [35, 45] and radial basis functions [34]. In this paper, we use Lagrange basis functions, moving least-squares (MLS) approximants and non-uniform rational B-splines (NURBS) to approximate the unknown field variables. The response of such low-dimensional structures is studied with the framework of the Galerkin method. The influence of the nonlocal parameter, boundary conditions, the aspect ratio and the plate dimensions on the fundamental frequency and the critical buckling load is numerically studied. The longitudinal vibration of a nanorod with a crack is also studied within the framework of the extended finite element method (XFEM).

1.3 Outline

The paper commences with a brief overview of Eringen's nonlocal elasticity theory and Aifantis' gradient elasticity theory. Section 3 presents the governing equations for nanobeams and nanoplates based on Eringen's gradient elasticity theory. The weak form of the corresponding equations is also described. The section also discusses the application of the partition of unity methods (PUMs) and the choice of various basis functions to describe the unknown field variables within nonlocal elasticity theory. Section 4 presents numerical results for longitudinal and free flexural vibration of nanobeams and nanoplates. The critical buckling load of a nanobeam is also studied. Concluding remarks are presented in the last section.

2 Overview of Eringen's nonlocal elasticity theory and Aifantis' gradient elasticity theory

Consider a region Ω in three-dimensional Euclidean space occupied by a continuum body. The body can be envisioned as a collection of a large number of deformable particles. If the internal motion of the particle is neglected and if a single typical material particle is assumed to interact with its neighbors with short-range elastic forces, the resulting theory is the "local elasticity theory", whereas in the "nonlocal elasticity theory", all the particles which influence one another are considered to write out the stress-strain relations. In this section, we discuss two types of nonlocal elasticity theory, namely Eringen's nonlocal elasticity theory and Aifantis' gradient elasticity theory. Both theories require only one additional parameter to be calibrated.

2.1 Eringen's nonlocal elasticity theory

Eringen [11, 12] by accounting for long-range cohesive forces proposed a nonlocal theory in which the stress at a point depends on the strains of an extended region around that point in the body. Thus, the nonlocal stress tensor σ at a point $\mathbf{x}$ is expressed as

$$\boldsymbol{\sigma}=\int_{\Omega}\alpha(|\mathbf{x}'-\mathbf{x}|)\mathbf{t}(\mathbf{x}')\,\mathrm{d}\mathbf{x}', \tag{1}$$

where $\mathbf{t}(\mathbf{x})$ is the classical, macroscopic stress tensor at a point $\mathbf{x}$ and the kernel function is called the nonlocal modulus, also referred to as the attenuation or influence function. The nonlocality effects at a reference point $\mathbf{x}$ produced by the strains at $\mathbf{x}$ and $\mathbf{x}'$ are included in the constitutive law by this function. The kernel weights the effects of the surrounding stress states. From the structure of the nonlocal constitutive equation, given by Eq. (1), it can be seen that the nonlocal modulus has the dimension of $(\text{length})^{-3}$ [11, 12]. Typically, the kernel is a function of the Euclidean distance between the points $\mathbf{x}$ and $\mathbf{x}'$. The kernel in Eq. (1) has the following properties:

1. The kernel is maximum at $\mathbf{x}'=\mathbf{x}$ and decays with $|\mathbf{x}'-\mathbf{x}|$.
2. The classical elasticity limit is recovered in the limit of the vanishing internal characteristic length $\lim_{\tau\to 0}\alpha(|\mathbf{x}'-\mathbf{x}|)=\delta(|\mathbf{x}'-\mathbf{x}|)$.
3. For small internal characteristic lengths, the nonlocal theory approximates the atomic lattice dynamics.
4. The kernel is a Green's function of a linear differential operator $\mathbf{L}$, $\mathbf{L}\alpha(|\mathbf{x}'-\mathbf{x}|)=\delta(|\mathbf{x}'-\mathbf{x}|)$.

The nonlocal modulus has a very important role in describing nonlocal effects. Of course, ultimately, the accurate estimation of $\alpha(|\mathbf{x}'-\mathbf{x}|)$ would dictate the overall reliability of the nonlocal model. Eringen [11, 12] numerically determined the functional form of the kernel. This is feasible due to the Cauchy-Born rule [46–48], which states that in a medium subjected to a small strain, the position of the atoms follows the overall strain of the medium. This rule, in general, can be applied directly to face-centered and body-centered cubic systems and, with slight modification, also to more complex lattices such as the diamond. Eringen [10] showed that a stress gradient theory can be derived by assuming that the nonlocal kernel is a special form that satisfies the differential equation

$$[1-\mu\nabla^2]\alpha(|\mathbf{x}'-\mathbf{x}|)=\delta(|\mathbf{x}'-\mathbf{x}|), \tag{2}$$

where $\mu=(e_0 a/L)^2$ is a material-specific parameter, called the nonlocal parameter, a is an internal characteristic parameter, L is the macroscopic length and e_0 is a constant. In such a stress gradient type of nonlocal elasticity theory, the relevant constitutive equation is given by

$$[1-\mu\nabla^2]\boldsymbol{\sigma}=\mathbf{D}\boldsymbol{\varepsilon}, \tag{3}$$

where $\mathbf{D}$ is the fourth-order elasticity tensor and ε is the local strain tensor.

2.2 Aifantis' gradient elasticity theory

In gradient-type nonlocal elasticity theory, the stress is expressed as a function of strain and its gradients at the same point [3]. In this category, there are two classes of strain gradient elasticity models:

Gradient theory type I: The gradient elasticity model in which the higher order term has been postulated and which is used to smoothen heterogeneity. The constitutive equation in this type is given by [3]

$$\boldsymbol{\sigma}=\mathbf{D}[1-\mu\nabla^2]\boldsymbol{\varepsilon}. \tag{4}$$

Gradient theory type II: The gradient elasticity model derived from a discrete lattice structure and which is used to introduce heterogeneity. The constitutive equation is given by

$$\boldsymbol{\sigma}=\mathbf{D}[1+\mu\nabla^2]\boldsymbol{\varepsilon}. \tag{5}$$

Remark 1: The only difference between these two classes of the gradient elasticity model is the "sign" of the higher order terms.

More details on Aifantis' strain gradient elasticity model and its use to interpret size effects eliminate stress/strain singularities from dislocation lines and crack tips can be found in a series of articles by Aifantis and coworkers [49–61], as well as references quoted therein. In these references, a comparison of fundamental differences between Eringen's stress gradient theory and Aifantis' strain gradient theory can be found. In the following, we mainly apply Eringen's model to study the static and dynamic behavior of low-dimensional structures. Aifantis' theory for such structures is considered separately elsewhere.

3 Governing equations based on Eringen's nonlocal elasticity and choice of basis functions

3.1 Governing equations

In this section, we present the governing equations for nanorods, nanobeams and nanoplates based on Eringen's differential stress gradient elasticity. For more information and detailed derivation, interested readers are referred to the literature [17, 39] and references therein.

3.1.1 Nanorods

For nanorods, the constitutive relation is given by

$$N-\mu\frac{\partial^2 N}{\partial x^2}=\mathrm{EA}\frac{\partial u}{\partial x}, \tag{6}$$

where N is the stress resultant, EA is the effective axial rigidity and u is the axial displacement. The equation of motion for the axial vibration of the nanorod is given by

$$\frac{\partial}{\partial x}\left(\mathrm{EA}\frac{\partial u}{\partial x}\right)=\left(1-\mu\frac{\partial^2}{\partial x^2}\right)\rho\frac{\partial^2 u}{\partial t^2}. \tag{7}$$

3.1.2 Timoshenko beam theory

Consider a straight uniform beam of length L and thickness h. The displacement field is given by

$$u(x,z,t)=u_0(x,t)+z\phi(x,t);\quad w(x,z,t)=w_0(x,t), \tag{8}$$

where u_0 and w_0 are the axial and the transverse displacements of the point on the mid-plane (i.e., $z=0$) of the beam and ϕ is the rotation of the mid-plane. The non-zero strains are

$$\varepsilon_{xx}=\frac{\partial u_0}{\partial x}+z\frac{\partial \phi}{\partial x};\quad \gamma_{xz}=\frac{\partial w_0}{\partial x}+\phi. \tag{9}$$

The Timoshenko beam theory requires shear correction factors to compensate for the error due to the constant shear stress assumption. The governing equations of motion in this case are given by

$$[GA\kappa_s(\phi+w_{,x})]_{,x}+q-(\bar{N}w_{,x})_{,x}-\mu[q-(\bar{N}w_{,x})_{,x}]_{,x} =m_0(\ddot{w}-\mu\ddot{w}_{,xx}) \tag{10a}$$

$$(EI\phi_{,x})_{,x}-GA\kappa_s(\phi+w_{,x})=m_1(\ddot{\phi}-\mu\ddot{\phi}_{,xx}), \tag{10b}$$

where the subscript "comma" denotes partial derivative with respect to the spatial coordinate succeeding it, G is the shear modulus, κ_s is the shear correction factor, q is the externally applied load, m_0 and m_1 are the mass densities, EI is the flexural rigidity and $\bar{N}$ is the externally applied axial load. The boundary conditions involve specifying one of each of the following at $x=0$ and at $x=L$: w or Q and ϕ or M, where Q is the shear force and M is the bending moment.

3.1.3 Reissner-Mindlin plates

Consider a rectangular Cartesian coordinate system (x, y, z) with the xy-plane coinciding with the undeformed middle plane of the plate and the z-coordinate taken positive downwards. The displacement field based on the first-order shear deformation theory, also referred to as the Reissner-Mindlin plate theory, is given by

$$\begin{aligned} u(x,y,z,t)&=u_0(x,y,t)+z\theta_x(x,y,t)\\ v(x,y,z,t)&=v_0(x,y,t)+z\theta_y(x,y,t)\\ w(x,y,z,t)&=w_0(x,y,t), \end{aligned} \tag{11}$$

where u_0, v_0 and w_0 are the mid-plane displacements and θ_x and θ_y are the rotations of the mid-plane. The strains are given by

$$\boldsymbol{\varepsilon}=\begin{Bmatrix}\boldsymbol{\varepsilon}_p\\0\end{Bmatrix}+\begin{Bmatrix}z\boldsymbol{\varepsilon}_b\\\boldsymbol{\varepsilon}_s\end{Bmatrix}. \tag{12}$$

The mid-plane strains, the bending strains and the shear strains in Eq. (12) are written as

$$\boldsymbol{\varepsilon}_p=\begin{Bmatrix}u_{0,x}\\v_{0,y}\\u_{0,y}+v_{0,x}\end{Bmatrix} \tag{13a}$$

$$\boldsymbol{\varepsilon}_b=\begin{Bmatrix}\theta_{x,x}\\\theta_{y,y}\\\theta_{x,y}+\theta_{y,x}\end{Bmatrix} \tag{13b}$$

$$\boldsymbol{\varepsilon}_s=\begin{Bmatrix}\theta_x+w_{0,x}\\\theta_y+w_{0,y}\end{Bmatrix}. \tag{13c}$$

The equations of motion are given by

$$\frac{\partial N_{xx}}{\partial x}+\frac{\partial N_{xy}}{\partial x}=I_{11}\ddot{u}+I_{12}\ddot{\theta}_x \tag{14a}$$

$$\frac{\partial N_{xy}}{\partial x}+\frac{\partial N_{yy}}{\partial x}=I_{11}\ddot{v}+I_{12}\ddot{\theta}_y \tag{14b}$$

$$\frac{\partial N_{xz}}{\partial x}+\frac{\partial N_{yz}}{\partial x}=I_{11}\ddot{w} \tag{14c}$$

$$\frac{\partial M_{xx}}{\partial x}+\frac{\partial M_{xy}}{\partial x}=I_{12}\ddot{u}+I_{22}\ddot{\theta}_x \tag{14d}$$

$$\frac{\partial M_{xy}}{\partial x}+\frac{\partial M_{yy}}{\partial x}=I_{12}\ddot{v}+I_{22}\ddot{\theta}_y, \tag{14e}$$

where $(I_{11}, I_{12}, I_{22})=\int_{-h/2}^{h/2}\rho(1, z, z^2)\,\mathrm{d}z$. The relation between the nonlocal stress and moment resultants to its local counterpart is given by

$$[1-\mu\nabla^2]\begin{Bmatrix}N_{ij}\\M_{ij}\end{Bmatrix}=\begin{Bmatrix}N_{ij}^{\mathrm{L}}\\M_{ij}^{\mathrm{L}}\end{Bmatrix}. \tag{15}$$

The local stress and moment resultants are related to the strains by

$$\begin{Bmatrix}\mathbf{N}\\\mathbf{M}\end{Bmatrix}=\begin{bmatrix}\mathbf{A}_e & \mathbf{B}_{be}\\\mathbf{B}_{be} & \mathbf{D}_b\end{bmatrix}\begin{Bmatrix}\boldsymbol{\varepsilon}_b\\\kappa\end{Bmatrix} \tag{16}$$

where $\mathbf{A}$, $\mathbf{B}_{be}$ and $\mathbf{D}_b$ are the extensional, the bending-extensional coupling and the bending stiffness coefficients, respectively. The equations of motion in terms of the mid-plane displacements and rotations are obtained by substituting the nonlocal (strictly speaking gradient) constitutive relations given by Eq. (16) into the equations of motion given by Eq. (14) along with Eq. (15). For a detailed derivation, interested readers are referred to the literature [33, 36, 38].

Remark 2: The governing equations of motion for classical elasticity can be obtained by setting the nonlocal parameter μ equal to zero.

3.2 Discretized form

The standard Galerkin procedure can be adopted to derive the following discretized form of the governing equations of motion for nanorods, nanobeams and nanoplates.

$$\textit{vibration}: \mathbf{K}\boldsymbol{\delta}+\ddot{\boldsymbol{\delta}}(\mathbf{M}+\mathbf{M}^{\mathrm{NL}})=\mathbf{0} \tag{17}$$

$$\textit{Buckling}: (\mathbf{K}+\lambda[\mathbf{K}_G+\mathbf{K}_G^{\mathrm{NL}}])\boldsymbol{\delta}=\mathbf{0}, \tag{18}$$

where $\boldsymbol{\delta}$ is the vector of unknown field variables, λ is the critical buckling load, $\mathbf{K}$ is the stiffness matrix, $\mathbf{K}_G$ is the geometric stiffness matrix, $\mathbf{M}$ is the mass matrix and the superscript "NL" refers to the contribution from the nonlocal part. Note that when Eringen's stress gradient elasticity theory is employed, the nonlocal parameter influences only the mass matrix in the case of free vibration and the geometric stiffness matrix in the case of buckling. The stiffness matrix is unaltered. It is also noted that, for the free vibration problem, the approximation functions require only $\mathcal{C}^0$ continuity, whereas the approximation functions need to be $\mathcal{C}^1$ continuous for the buckling problem. The stiffness matrix and the mass matrix for nanobeams and nanoplates are given below.

3.2.1 Timoshenko beam

The elemental stiffness, the geometric stiffness and the elemental mass matrix for the nonlocal Timoshenko beam are given by

$$\mathbf{K}^e=\int_{\Omega^3}\mathbf{B}^{\mathrm{T}}\begin{bmatrix}EI & 0\\ 0 & GA\kappa_s\end{bmatrix}\mathbf{B}\,\mathrm{d}\Omega \tag{19a}$$

$$\mathbf{M}^e=\int_{\Omega^e}\mathbf{N}^{\mathrm{T}}\begin{bmatrix}\rho A & 0\\ 0 & \rho I\end{bmatrix}\mathbf{N}\,\mathrm{d}\Omega+\mu\mathbf{N}_{,x}^{\mathrm{T}}\begin{bmatrix}\rho A & 0\\ 0 & \rho I\end{bmatrix}\mathbf{N}_{,x}\,\mathrm{d}\Omega. \tag{19b}$$

$$\mathbf{K}_G^e=\int_{\Omega^e}\mathbf{N}^{\mathrm{T}}\left(\frac{\partial\mathbf{N}^2}{\partial x^2}\right)^T\frac{\partial\mathbf{N}^2}{\partial x^2}(1+\mu)\,\mathrm{d}\Omega. \tag{19c}$$

Remark 3: It is seen from the above equations that the computation of the geometric stiffness matrix involves the second derivative of the approximation functions, i.e., the approximation functions should be $\mathcal{C}^1$ continuous.

3.2.2 Reissner-Mindlin plate

The elemental stiffness and mass matrix for the nonlocal stress gradient Reissner-Mindlin plate are given by

$$\mathbf{K}^e=\int_{\Omega^e}\left(\mathbf{B}^{\mathrm{T}}\begin{bmatrix}\mathbf{A}_e & \mathbf{B}_{be}\\ \mathbf{B}_{be} & \mathbf{D}_b\end{bmatrix}\mathbf{B}+\mathbf{B}_s^{\mathrm{T}}\mathbf{E}\mathbf{B}_s\right)\mathrm{d}\Omega \tag{20a}$$

$$\mathbf{M}^e=\int_{\Omega^e}\mathbf{N}^{\mathrm{T}}\rho\begin{bmatrix}h & 0 & 0 & 0 & 0\\ 0 & h & 0 & 0 & 0\\ 0 & 0 & h^3/12 & 0 & 0\\ 0 & 0 & 0 & h^3/12 & 0\\ 0 & 0 & 0 & 0 & h^3/12\end{bmatrix}\mathbf{N}\,\mathrm{d}\Omega \tag{20b}$$

$$\mathbf{M}_{\mathrm{NL}}^e=\int_{\Omega^e}\frac{\partial\mathbf{N}^{\mathrm{T}}}{\partial\eta}\rho\mu\begin{bmatrix}h & 0 & 0 & 0 & 0\\ 0 & h & 0 & 0 & 0\\ 0 & 0 & h^3/12 & 0 & 0\\ 0 & 0 & 0 & h^3/12 & 0\\ 0 & 0 & 0 & 0 & h^3/12\end{bmatrix}\frac{\partial\mathbf{N}}{\partial\eta}\mathrm{d}\Omega, \tag{20c}$$

where $\eta=x, y$ and $\mathbf{B}$ and $\mathbf{B}_s$ are the strain-displacement matrices corresponding to bending-extensional coupling and shear terms, respectively.

3.3 Choice of basis functions

As noted earlier, the numerical implementation of the nonlocal or the gradient elasticity theory requires at least $\mathcal{C}^1$ continuous functions in some cases, for example, buckling. For this, the conventional finite element approach with Lagrange polynomials is not suitable. In this section, we discuss the different choices of basis functions.

3.3.1 $\mathcal{C}^1$ finite elements

The higher order gradients of strain and stresses in Aifantis' gradient elasticity and Eringen's gradient elasticity theory, respectively, lead to partial differential equations of higher order. Employing Galerkin's method for numerical solution requires a high regularity of the interpolation scheme. For the first-order strain gradient theory, $\mathcal{C}^1$ continuity has to be ensured. There are only a limited number of $\mathcal{C}^1$ continuous finite elements. The Argyris element, the bicubic element and the HCT element have been used in the literature for gradient elasticity problems. All these elements satisfy $\mathcal{C}^1$ continuity requirement imposed by the gradient elasticity formulation. Figure 1 shows the first six shape functions for a triangular element with three nodes. Each node has six degrees of freedom, i.e., u, u_x, u_y, u_{xx}, u_{xy} and u_{yy}. The explicit form of the shape functions is given in [62]. These elements have many degrees of freedom per node and are difficult to implement. Papaconstantopoulos et al. [63] developed a three-dimensional hexahedral element with $\mathcal{C}^1$ continuity. In [19], Hermite interpolation functions and Hermite cubic elements were

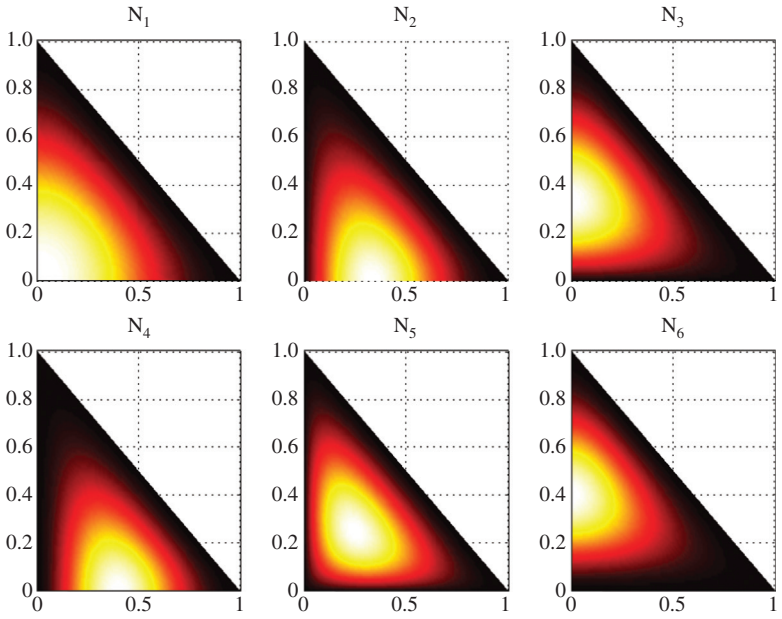

Figure 1 C^1 shape functions for a triangular finite element. Only the first six shape functions corresponding to a node are shown. The other shape functions can be constructed by permutation [62].

employed for studying static and dynamic characteristics of nonlocal Euler-Bernoulli beams and nonlocal Kirchoff plates, respectively. The Hermite cubic element involves a 12-term approximation polynomial with $\left(w, \frac{\partial w}{\partial x}, \frac{\partial w}{\partial y}\right)$ as the nodal degrees of freedom, where w is the transverse displacement.

3.3.2 Non-uniform rational B-splines

NURBS is a short form for non-uniform rational B-splines. We give here only a brief introduction to NURBS. More details on their use in FEM are given in [64, 65]. The key ingredients in the construction of NURBS basis functions are the knot vector (a non-decreasing sequence of parameter values, $\xi_i \le \xi_{i+1}$, i=0, 1, ..., m–1), the control points, P_i, the degree of the curve p and the weight associated with a control point, w. The i_{th} B-spline basis function of degree p, denoted by $N_{i,p}$ is defined as [66]

$$N_{i,0}(\xi) = \begin{cases} 1 & \text{if } \xi_i \le \xi \le \xi_{i+1} \\ 0 & \text{else} \end{cases} \tag{21a}$$

$$N_{i,p}(\xi) = \frac{\xi - \xi_i}{\xi_{i+p} - \xi_i} N_{i,p-1}(\xi) + \frac{\xi_{i+p+1} - \xi}{\xi_{i+p+1} - \xi_{i+1}} N_{i+1,p-1}(\xi). \tag{21b}$$

The B-spline basis functions have the following properties: (i) non-negativity, (ii) partition of unity, $\sum_i N_{i,p} = 1$ and (iii) interpolatory at the end points. As the same function is also used to represent the geometry, the exact representation of the geometry is preserved. It should be noted that the continuity of the spline functions can be tailored to the needs of the problem. Moreover, the spline function has limited support. When employed to approximate the FE solution space, the resulting stiffness matrix has similar properties to the stiffness matrix computed by employing Lagrange shape functions. Given n+1 control points ($\mathbf{p}_0$, $\mathbf{p}_1$, ..., $\mathbf{p}_n$) and a knot vector $\Xi = \{\eta_0, \eta_1, ..., \eta_m\}$, the piecewise polynomial B-spline curve of degree p is defined as

$$\mathbf{C}(\eta) = \sum_{i=0}^{n} \mathbf{P}_i N_{i,p}(\eta), \tag{22}$$

where $\mathbf{P}_i$ are the control points. A B-spline curve has the following information: n+1 control points, m+1 knots and a degree p. It is noted that n, m and p must satisfy $m = n + p + 1$. The B-spline functions also provide a variety of refinement algorithms, which are essential when employing B-spline functions to discretize the unknown fields. The analogous h and p refinement can be done by the process of "knot insertion" and "order elevation". The B-spline surfaces are defined by the tensor product of basis functions in two parametric dimensions ξ and η with two knot vectors, one in each dimension as

$$\mathbf{C}(\xi, \eta) = \sum_{i=1}^{n} \sum_{j=1}^{m} N_{i,p}(\xi) M_{j,q}(\eta) \mathbf{P}_{i,j}, \tag{23}$$

where $\mathbf{P}_{i,j}$ is the bidirectional control net and $N_{i,p}$ and $M_{j,q}$ are the B-spline basis functions defined on the knot vectors over an $m\times n$ net of control points $\mathbf{P}_{i,j}$. Despite the flexibility offered by the B-splines, they lack the ability to exactly represent some shapes such as circles and ellipsoids. To improve this, NURBS are formed through rational functions of B-splines. The NURBS thus form the superset of B-splines. The key ingredients in the construction of NURBS basis functions are the knot vector (a non-decreasing sequence of parameter values, $\eta_i \leq \eta_{i+1}$, i=0, 1, ..., m–1), the degree of the curve p and the weight associated with a control point, w. A pth degree NURBS basis function is defined as follows:

$$R(\eta)=\frac{N_{i,p}(\eta)w_i}{W(\eta)}=\frac{N_{i,p}(\eta)w_i}{\sum_{i=0}^{n}N_{i,p}(\eta)w_i}, \tag{24}$$

where w_i are the weights for the ith basis function $N_{i,p}(\eta)$. Figure 2 shows the third-order NURBS for an open knot vector Ξ={0, 0, 0, 0, 1/3, 1/3, 1, /3, 1/2, 2/3, 1, 1, 1, 1}.

The NURBS surface is then defined by

$$\mathbf{R}(\xi,\eta)=\frac{\sum_{i=1}^{n}\sum_{j=1}^{m}N_{i,p}(\xi)M_{j,q}(\eta)\mathbf{P}_{i,j}w_i w_j}{w(\xi,\eta)}, \tag{25}$$

where $w(\xi, \eta)$ is the weighting function. The displacement field, $\mathbf{u}_\tau(x, y)$ within the control mesh is approximated by

$$\mathbf{u}_\tau(x,y)=\mathbf{R}(\xi,\eta)\mathbf{q}_\tau(x,y), \tag{26}$$

where $\mathbf{q}_\tau(x, y)$ are the nodal variables and $\mathbf{R}(\xi, \eta)$ are the basis functions given by Eq. (25).

3.3.3 MLS approximants

The unknown field variables can be approximated by the MLS approximation as

$$\mathbf{u}^h(\mathbf{x})\equiv\mathbf{p}^{\mathrm{T}}(\mathbf{x})\mathbf{a}(\mathbf{x}), \tag{27}$$

where $\mathbf{p}(\mathbf{x})$ is a vector of basis functions and $\mathbf{a}(\mathbf{x})$ are unknown coefficients. The unknown coefficients $\mathbf{a}(\mathbf{x})$ are obtained by minimizing a weighted least-squares sum of the difference between the local approximation $\mathbf{u}^h(\mathbf{x})$ and the field function nodal parameters $\mathbf{u}_I$. The weighted least-squares sum $L(\mathbf{x})$ can be written in the quadratic form as

$$L(\mathbf{x})=\sum_{i=1}^{n}w(\mathbf{x}-\mathbf{x}_I)[\mathbf{p}^{\mathrm{T}}(\mathbf{x})\mathbf{a}(\mathbf{x})-\mathbf{u}_I]^2, \tag{28}$$

where $\mathbf{u}_I$ is the nodal parameter associated with node I at $\mathbf{x}_I$, $w(\mathbf{x}-\mathbf{x}_I)$ is the weight function having a compact support associated with node I and n is the total number of nodes with the domain of influence containing the points $\mathbf{x}$ where $w(\mathbf{x}-\mathbf{x}_I)\neq 0$. By setting $\partial L/\partial\mathbf{a}=0$, we obtain the following set of linear equations:

$$\mathbf{A}(\mathbf{x})\mathbf{a}(\mathbf{x})=\mathbf{B}(\mathbf{x})\mathbf{u}. \tag{29}$$

Upon substituting Eq. (26) into Eq. (24), we obtain the approximation function as

$$\mathbf{u}^h(\mathbf{x})\equiv\sum_{i=1}^{n}\Phi_I(\mathbf{x})\mathbf{u}_I. \tag{30}$$

Figure 3 shows a typical MLS function with a quartic spline weight function. Note that the MLS shape functions

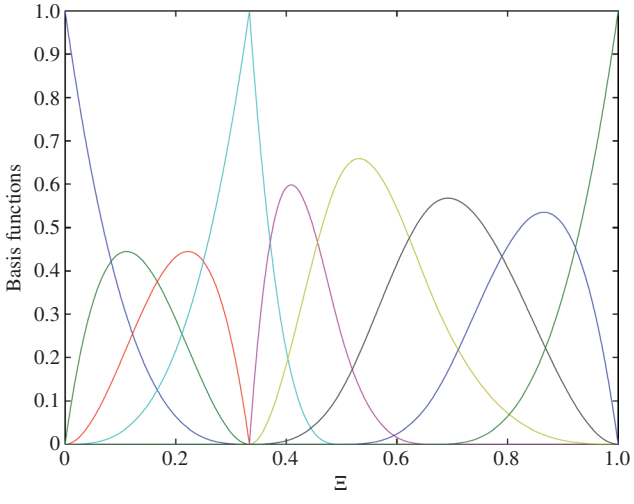

Figure 2 Non-uniform rational B-splines. Order of the basis function is 3 with the open knot vector.

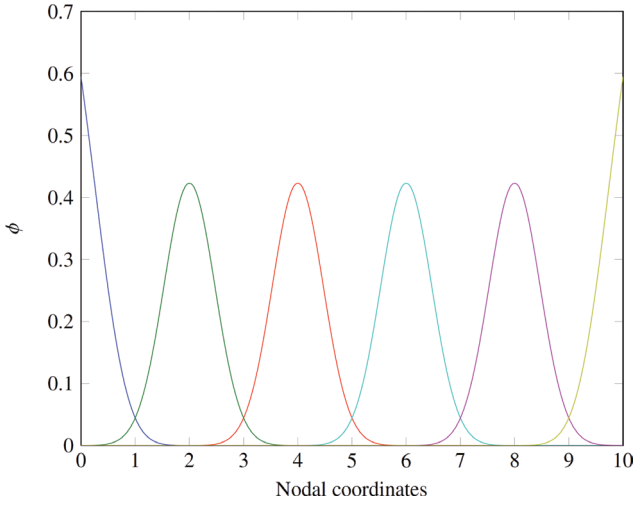

Figure 3 Moving least-squares basis function with the quartic spline weight function.

do not satisfy the Kronecker delta property, and hence imposing boundary conditions requires an additional step. However, the MLS shape functions satisfy the partition of unity property, which makes them a candidate as basis functions within the Galerkin procedure. Moreover, the higher order continuity of the shape functions can be constructed.

Remark 4: When applying the NURBS or MLS approximations for gradient elasticity, the inherent higher order continuity of the shape functions is utilized.

3.3.4 Field-consistent Q4 and Q8 elements

In order to study the free vibration of Reissner-Mindlin plates, we employ four-noded and eight-noded shear flexible quadrilateral elements. These plate elements are C^0 continuous elements with five degrees of freedom per node. The same element can be used within the nonlocal elasticity framework to study the free vibration of nanoplates, because the weak form (Eq. 21) does not involve higher order derivatives of the shape functions. However, if the interpolation functions for Q4/Q8 are used directly to interpolate the five variables in deriving the shear strains and membrane strains, the element will lock and show oscillations in the shear and membrane stresses. Field consistency requires that the transverse shear strains and membrane strains must be interpolated in a consistent manner. Thus, the θ_x and θ_y terms in the expressions for shear strains ε_s have to be consistent with the derivatives of the field functions $w_{0,x}$ and $w_{0,y}$. This is achieved by using field redistributed substitute shape functions to interpolate these specific terms, which must be consistent as described in [66, 67]. These elements are free from locking and have good convergence properties. For a complete description of the element, interested readers are referred to the literature [66, 67], where the element behavior is discussed in great detail. Since the element is based on the field consistency approach, exact integration is applied for calculating various strain energy terms.

4 Numerical results and discussion

In this section, we study the nonlocal response of low-dimensional structures using the PUMs. For all the study, consistent units are used for the material properties.

4.1 Axial vibration of nanorods

In this section, we study the influence of the internal length μ, boundary conditions and the presence of a crack on the fundamental frequency of a nanorod. The nanorod with length L has Young's modulus E and uniform cross-section A. The crack is located at a distance C from the left end and it is simulated by an equivalent spring with stiffness k. In this work, the influence of a single crack on the longitudinal vibration is studied. In this example, we represent the discontinuity (i.e., crack) independently of the mesh within the framework of the XFEM. Within this framework, the generic form of the displacement approximation is given by

$$\mathbf{u}^h = \sum_{I\in\mathcal{N}^{\text{fem}}} N_I(\mathbf{x})\mathbf{q}_I + \sum_{J\in\mathcal{N}^{\text{xfem}}} N_J(\mathbf{x})\varrho(\mathbf{x})\mathbf{a}_J, \tag{31}$$

where N_I, N_J are the standard finite element shape functions, $\mathcal{N}^{\text{fem}}$ is the set of nodes in the finite element mesh and $\mathcal{N}^{\text{xfem}}$ is the set of nodes whose nodal support is cut by the discontinuity. Interested readers are referred to [68] for more details. The weak form is given by

$$\int_\Omega \nabla:\boldsymbol{\sigma}\,\mathrm{d}\Omega + \int_{\Gamma_{\text{coh}}} \mathbf{t}_c\cdot\mathbb{U}\,\mathrm{d}\Gamma = \int_{\Gamma_t} \bar{\mathbf{t}}\cdot w\,\mathrm{d}\Gamma, \tag{32}$$

where $\mathbb{U}=\mathbf{u}\cdot\mathbf{n}, \mathbf{t}_c=\mathbf{t}_c\cdot\mathbf{n}$ and $\mathbf{t}_c=ku$; k is the spring stiffness.

Before proceeding further with the numerical study, the results from the present formulation are compared with results available in the literature for the case when the nonlocal parameter $\mu=0$. Based on a progressive mesh refinement, 100 elements were found to be adequate for the study. Figure 4 shows the convergence of the first three modes with mesh size with and without nonlocal effects. It can be seen that with decreasing mesh size, the analytical solution is approached.

Tables 1 and 2 give a comparison of computed frequencies for the clamped-free (CF) and clamped-clamped (CC) nanobeam with a single crack, respectively [69, 70]. It can be seen that the numerical results from the present formulation are found to be in good agreement with the existing previous solutions. The effect of the nonlocal parameter on the fundamental frequencies is shown in Figure 5 for a fixed value of the nonlocal parameter (e_0a=1 nm). In this case, the length of the beam is varied. It can be seen that as the length of the beam increases with respect to the characteristic internal length, the nonlocal effect decreases, and for very large beams, the nonlocal effect is negligible.

Figure 6 depicts the influence of boundary conditions and nonlocal parameter on the first three models of the CF and CC beam with a single crack. The crack is

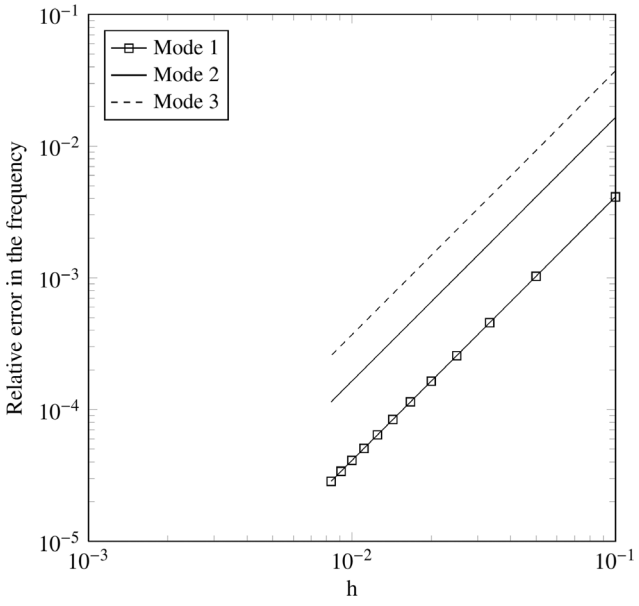

Figure 4 Convergence of the first three modes of frequencies with mesh size.

Table 1 Comparison of natural frequencies of the clamped-free beam with a single crack at C/L=0.2002, crack parameter $K=EA/kL$=0.1144 and nonlocal parameter e_0a/L=0.

Mode	XFEM	Ref. [69]	Ref. [70]
1	1.4228	1.4278	1.4278
2	4.4429	4.5579	4.5576
3	7.8559	7.8540	7.8540
4	10.4289	10.4471	10.4486

Table 2 Comparison of natural frequencies for the clamped-clamped beam with a single crack located at C/L=0.25 for various internal lengths and crack parameters.

$\mu=(e_0a/L)$	K=0.065		K=0.35		K=2	
	XFEM	Ref. [69]	XFEM	Ref. [69]	XFEM	Ref. [69]
0.2	2.6144	2.6173	2.4649	2.4668	2.1503	2.1506
0.4	1.9455	1.9467	1.9060	1.9071	1.7660	1.7663

located at C/L=0.4 from the left end. It can be seen that the frequencies are higher for the beam with no crack, and with increasing crack parameter $K=EA/kL$, the frequency decreases. The presence of crack introduces local flexibility, and the effect of the crack parameter on the frequencies is significant for lower values of the nonlocal parameter μ. This observation is consistent with the existing previous results [69]. The effect of crack local along the length of the beam and the boundary conditions on the frequency is shown in Figure 7. In both cases, the natural frequency

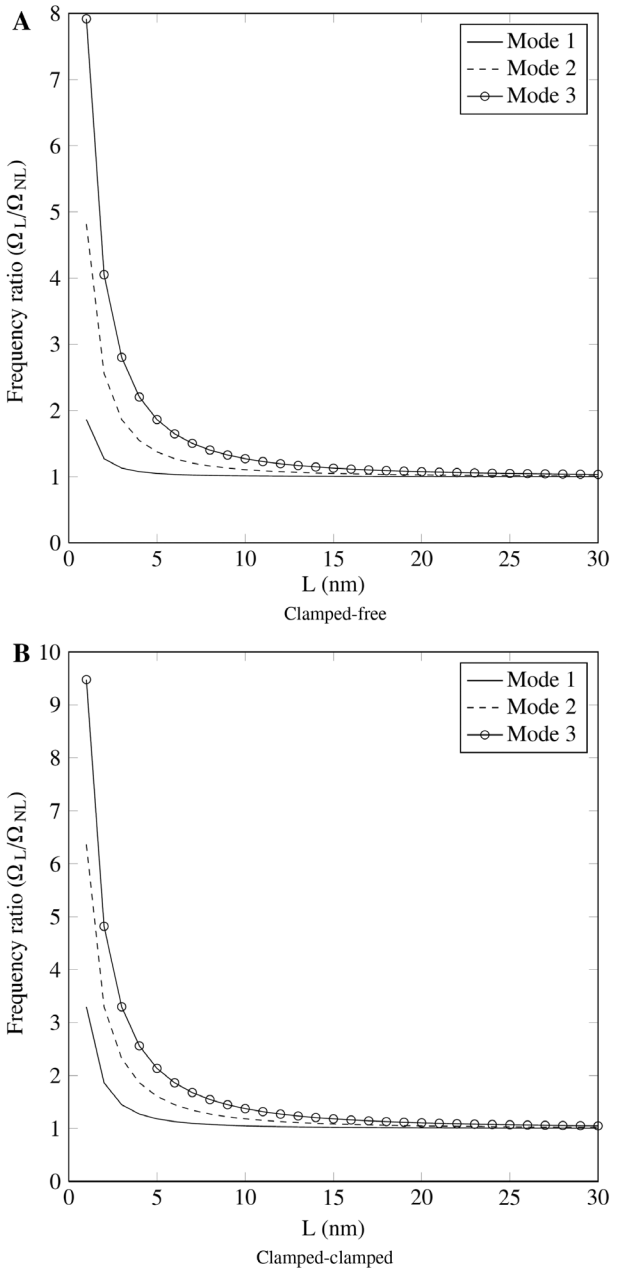

Figure 5 Frequency ratio β as a function of the beam length with a fixed nonlocal parameter e_0a=1 nm. It can be seen that as the length of the beam increases with respect to the characteristic internal length, the nonlocal effect decreases, and for very long beams, the nonlocal effect is negligible.

of the beam is influenced by the location of the crack. In the case of the CF boundary condition, the crack near the free end shows a stronger influence than the crack at the fixed end, whereas in the case of the CC boundary condition, the crack in the middle of the beam has a stronger influence. Due to the CC boundary condition, a symmetric distribution of the frequency is observed. This again is consistent with the results available in the literature [69].

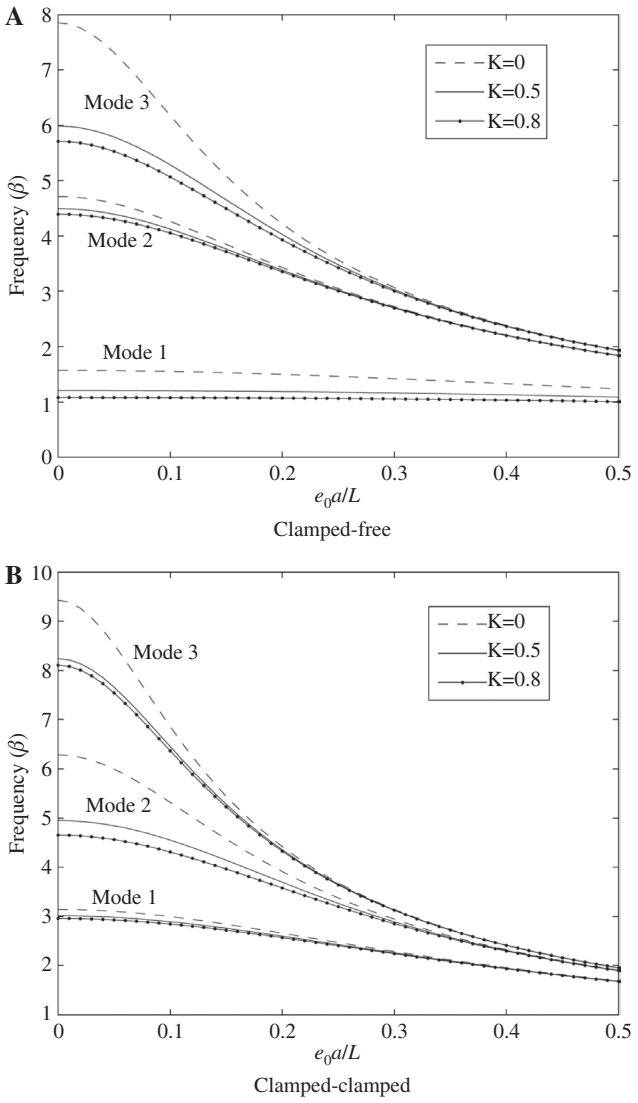

Figure 6 The dimensionless frequency for different crack parameters for the first three vibration modes. The crack is located at a distance 0.4 from the left end.

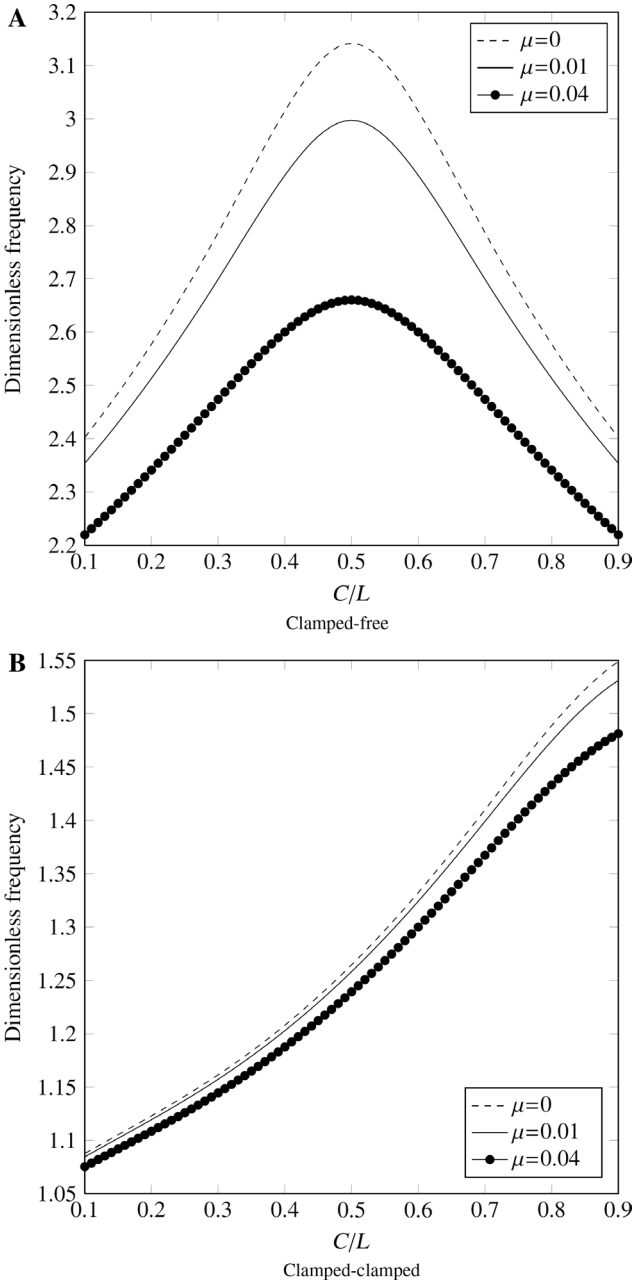

Figure 7 Influence of the crack location on the fundamental frequency for clamped-free and clamped-clamped nanorods for various internal lengths μ.

4.2 Flexural vibration and buckling of beams

In this section, we present the influence of the internal length on the fundamental frequencies and on the critical buckling load for nanobeams based on both Euler-Bernoulli beam and Timoshenko beam theories. In all cases, we present the non-dimensionalized fundamental frequencies as (unless specified otherwise)

$$\Omega=\omega L^2\sqrt{\frac{\rho}{EI}}, \tag{33}$$

where EI is the flexural rigidity, ρ is the mass density and L is the length of the beam.

4.2.1 Vibration of beams

Consider a beam of length L=10 with Young's modulus E=30×10⁶, Poisson's ratio ν=0.3 and mass density ρ=1. The influence of the beam thickness h, the nonlocal parameter μ and the boundary conditions [namely simply supported (SS) ends, CC and CF] on the fundamental frequency is numerically studied. The efficiency and accuracy of different basis functions, namely Lagrange interpolants, MLS

Table 3 Comparison of natural frequencies for the simply supported Timoshenko beam.

a/h	μ	Timoshenko beam				
		Ref. [17]	Ref. [34]	NURBS	MLS	FEM
100	0	9.8683	9.8283	9.8680	9.8645	9.8630
	1	9.4147	9.3766	9.4144	9.4112	9.4096
	2	8.0750	8.0423	8.0748	8.0725	8.0706
20	0	9.8381	9.8059	9.8281	9.8258	9.7955
	1	9.3858	9.3551	9.3763	9.3742	9.3452
	2	8.0503	8.0239	8.0421	8.0407	8.0154
10	0	9.7454	9.7792	9.7075	9.7034	9.5886
	1	9.2973	9.3294	9.2612	9.2538	9.1460
	2	7.9744	8.0014	7.9434	7.9385	7.8445

approximants and NURBS basis functions, are critically studied. The numerical results for free vibration of beams based on the Timoshenko beam theory are given in Table 3. The results from the present study are compared with the available analytical solution [17] and with radial basis functions [34]. It can be seen that the numerical results from the present study are in very good agreement with the existing solutions. The influence of the internal length μ and the thickness is also shown in Table 3. The combined effect of increasing the plate thickness and the nonlocal parameter μ is to decrease the fundamental frequency. The influence of the beam aspect ratio and the nonlocal parameter on the frequency ratio $\beta=\Omega_{NL}/\Omega_L$ and on the fundamental frequency Ω_{NL} is shown in Figure 8. It can be observed that increasing the nonlocal parameter, for a fixed aspect ratio, decreases the frequency ratio. The nonlocal parameter has a greater influence on the higher modes. The variation of the frequency ratio for mode 1 is almost linear, whilst for higher modes, the frequency ratio is nonlinear. The effect of increasing the aspect ratio is to increase the frequency, whilst increasing the nonlocal parameter decreases the frequency. This is because increasing the aspect ratio increases the flexibility of the structure, and on the other hand, the nonlocal parameter decreases the flexibility. The effect of various boundary conditions on the fundamental frequency is presented in Table 4. For this example, a NURBS basis function of order 3 is employed. It is observed that the frequency decreases with increasing nonlocal parameter. The CC boundary condition increases the fundamental frequency, whilst the CF lowers the frequency compared to the SS boundary condition.

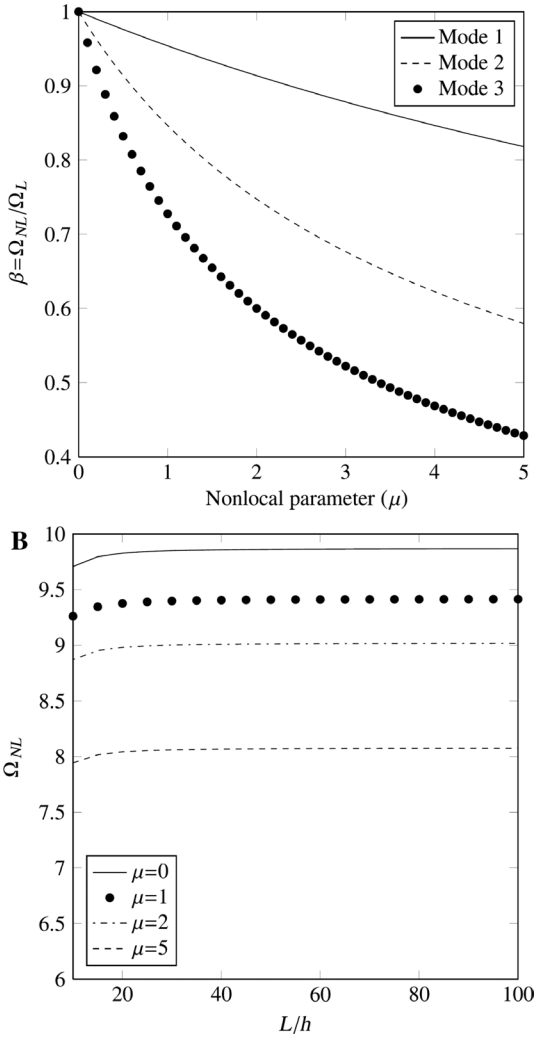

Figure 8 Timoshenko beam theory: (A) frequency ratio β as a function of the nonlocal parameter for a simply supported beam with a/h=100 and L=10 and (B) non-dimensionalized mode 1 frequency as a function of the aspect ratio L/h for various nonlocal parameters.

4.2.2 Buckling of beams

In this section, we present the critical buckling load for SS nanobeams based on the Timoshenko beam theory. For comparison purposes, we have included the results for nanobeams based on the Euler-Bernoulli beam theory. The non-dimensionalized critical buckling load is given by

$$\lambda^*=\bar{N}\frac{L^2}{EI}. \tag{34}$$

Consider a beam of length L=10 with Young's modulus $E=30\times10^6$ and Poisson's ratio ν=0.3. The weak form of the governing equations for nanobeam buckling requires $\mathcal{C}^1$ continuity, and hence we employ the element-free Galerkin method based on MLS approximants. The beam is discretized with 100 nodes with a quadratic polynomial basis and a quartic spline as a weight function. The non-dimensionalized critical buckling loads are presented in Table 5. From this table, it is observed that the buckling

Table 4 Non-dimensionalized frequency for the Timoshenko beam under various boundary conditions. Influence of the internal length and the aspect ratio is also shown.

a/h	μ	NURBS, p=3		
		SS	CC	CF
100	0	9.8680	22.3892	3.5178
	1	9.4144	21.1228	3.4385
	2	9.0180	20.0450	3.3639
	5	8.0748	17.5791	3.1646
20	0	9.8281	21.9967	3.5091
	1	9.3763	20.7595	3.4303
	2	8.9816	19.7049	3.3561
	5	8.0421	17.2877	3.1577
10	0	9.7075	20.9726	3.4884
	1	9.2612	19.8083	3.4107
	2	8.8713	18.8124	3.3375
	5	7.9434	16.5200	3.1415

load decreases with increasing nonlocal parameter μ. Similar to free vibration, for the shorter beam length L, the nonlocal effect is important, and this effect is negligible for longer beam lengths. The numerical results from the present study are compared with the results of Reddy [17] and very good agreement is observed. Moreover, it is noted that the influence of the nonlocal parameter does not depend on the beam theory used.

4.3 Free vibration of plates

In this section, we study the influence of the nonlocal parameter μ and the plate dimensions on the fundamental frequencies of rectangular and circular plates.

Table 5 Comparison of the critical buckling load for simply supported nanobeams.

Boundary condition	μ	Euler-Bernoulli beam		Timoshenko beam	
		Ref. [17]	MLS	Ref. [17]	MLS
SS	0.0	4.8458	4.8447	4.7670	4.7670
	0.5	4.7290	4.7281	4.6540	4.6540
	1.0	4.4105	4.4095	4.3450	4.3450
	1.5	3.9651	3.9644	3.9122	3.9121
	2.0	3.4741	3.4735	3.4333	3.4333
CF	0.0	1.2542	1.2112	1.2063	1.2063
	0.5	1.2062	1.2037	1.1989	1.1989
	1.0	1.1829	1.1820	1.1773	1.1773
	1.5	1.1593	1.1475	1.1431	1.1431
	2.0	1.1134	1.1024	1.0983	1.0983

4.3.1 Flat rectangular plate

Consider a plate of uniform thickness h, length a and width b. The following material properties are used: Young's modulus E=30×10^6, Poisson's ratio ν=0.3 and mass density ρ=1. In all cases, we present the non-dimensionalized free flexural frequency

$$\Omega=\omega h\sqrt{\frac{\rho}{D}}, \tag{35}$$

where $D=\frac{Eh^3}{12(1-\nu^2)}$ is the plate rigidity. In this case, the displacement field is approximated by Lagrange elements (Q4 and Q8) and with NURBS basis functions with each node having five degrees of freedom ($\boldsymbol{\delta}=u_0, v_0, w_0, \theta_x, \theta_y$). In this study, we employ a structured mesh size of 40×40 with Q4 elements, 8×8 with Q8 elements and cubic NURBS functions. The computed non-dimensionalized fundamental frequencies for a rectangular SS plate are given in Table 6. It can be seen that the numerical results from the present study are found to be in good agreement with the existing solutions. Table 6 gives the results of non-dimensional frequencies for a first-order nonlocal plate theory for different values of nonlocal parameters and aspect ratios for various basis functions. Again, it can be seen that the nonlocal theory predicts smaller values of natural frequencies than the local elasticity theory. The nonlocal frequency-to-local frequency ratio Ω_{NL}/Ω_L is computed for an SS isotropic square plate and the results are compared with those available in the literature [38]. Frequency ratios for different values of the nonlocal parameter are presented in Table 7. It can be seen that the results from the present formulation are in good agreement with the existing previous results [38, 39].

Table 6 Comparison of the non-dimensionalized fundamental frequency for a simply supported rectangular plate.

a/b	a/h	μ	Ref. [39]	Method		
				Q4	Q8	NURBS
1	10	0	0.0930	0.0927	0.0926	0.0929
		1	0.0850	0.0847	0.0846	0.0849
		5	0.0660	0.0657	0.0657	0.0659
	20	0	0.0239	0.0240	0.0238	0.0239
		1	0.0218	0.0219	0.0218	0.0219
		5	0.0169	0.0170	0.0169	0.0170
2	10	0	0.0589	0.0588	0.0587	0.0590
		1	0.0556	0.0554	0.0554	0.0556
		5	0.0463	0.0462	0.0462	0.0464
	20	0	0.0150	0.0150	0.0150	0.0151
		1	0.0141	0.0141	0.0141	0.0141
		5	0.0118	0.0118	0.0118	0.0118

Table 7 Comparison of the frequency ratio β for a simply supported square plate with a=10 and h=0.34. Consistent units are used for the study.

μ	Ref. [39]	Ref. [38]	Method		
			Q4	Q8	NURBS
0	1.0000	1.0000	1.0000	1.0000	1.0000
1	0.9139	0.9139	0.9099	0.9107	0.9107
2	0.8467	0.8467	0.8393	0.8468	0.8468
3	0.7925	0.7925	0.7857	0.7928	0.7928

Figure 9 shows the influence of plate dimensions and the influence of the internal length μ on the frequency ratio for an SS isotropic plate. The value of the nonlocal parameter is assumed to vary between μ=0 (local elasticity) and μ=3 nm^2 (nonlocal or stress gradient elasticity). It is seen that as the length of the plate increases for a fixed internal length μ, the frequency ratio tends to increase monotonically and approach the local elasticity solution for a considerably larger plate length, irrespective of the nonlocal parameter. The influence of the nonlocal parameter is significant for smaller plate dimensions. The influence of the nonlocal parameter on the frequency ratio for various plate dimensions is also shown in Figure 9. It can be seen that the nonlocal parameter has a stronger influence for small plate dimensions. The influence of the nonlocal parameter on the frequency ratio is nonlinear for small plate dimensions and the frequency ratio decreases with increasing nonlocal parameter. To study the influence of the nonlocal parameter and the boundary condition on the natural frequency of an isotropic plate, a square plate of length 10 nm is considered with a/h=100. The frequency ratio corresponding to two different boundary conditions, namely all edges SS and all edges clamped boundary conditions, is plotted in Figure 10. It can be seen that both the boundary condition and the nonlocal parameter have an influence on the frequency ratio. The higher the nonlocal parameter, the larger is the influence, irrespective of the boundary condition.

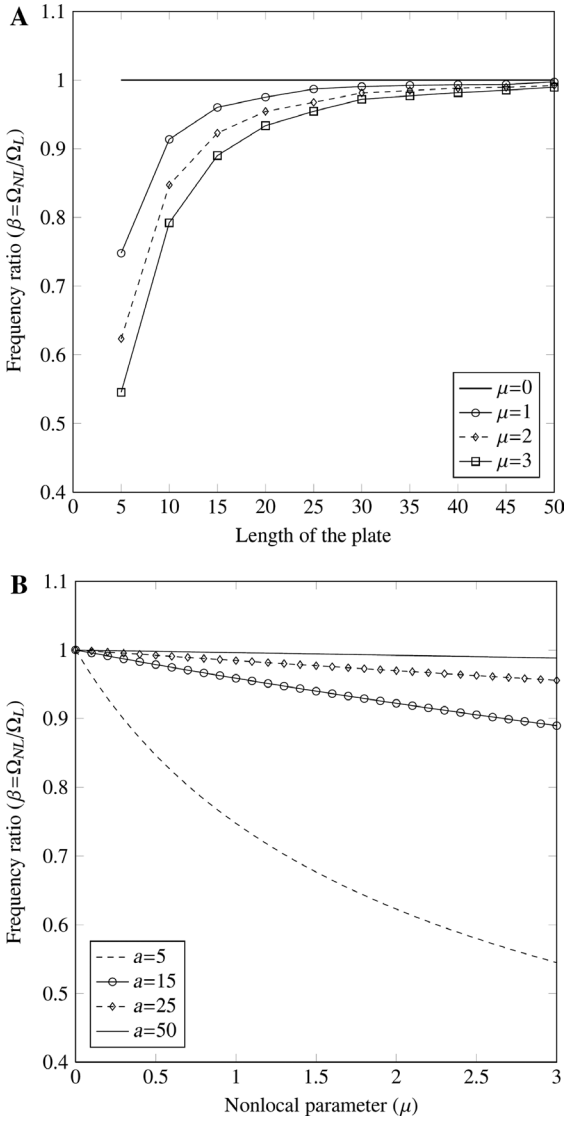

Figure 9 Frequency ratio β for a simply supported isotropic plate: (A) influence of the length of the plate for various internal lengths and (B) influence of the nonlocal parameter for various lengths of the plate.

4.3.2 Circular plate

In this example, we consider a circular plate with fully clamped boundary conditions. The following material

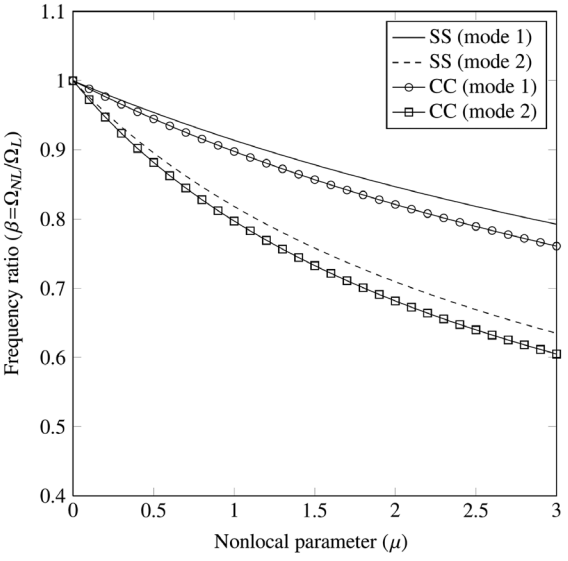

Figure 10 Frequency ratio as a function of the nonlocal parameter for various boundary conditions.

properties are used: Young's modulus E=205, Poisson's ratio ν=0.3 and mass density ρ=8900. The circular plate has a radius R=0.5. The influence of the radius-to-thickness ratio $\delta=h/R$ and the internal length μ on the fundamental frequency is numerically studied. In all cases, we present the non-dimensionalized free flexural frequency

$$\Omega=\omega R^2\sqrt{\frac{\rho h}{D}}. \tag{36}$$

For this problem, a NURBS quadratic basis function is sufficient to model exactly the circular geometry. Any further refinement, if done, will only improve the accuracy of the solution. The knot vectors for the coarsest mesh with one element are defined as follows: Ξ=[0,0,0,1,1,1] and $\mathcal{H}$=[0, 0, 0, 1, 1, 1]. The data for the circular plate are given in Table 8. Before proceeding further with details, the results from the present formulation are compared with available results pertaining to circulate plates based on the classical theory of elasticity. Table 9 presents the convergence of the first three fundamental frequencies with mesh refinement and order elevation. It can be seen that very good agreement with the available results is obtained and that the order elevation improves the accuracy of the solution. For the remainder of the analysis, 13×13 NURBS cubic elements are used. The influence of the radius-to-thickness ratio δ and the internal length μ on the fundamental frequency is presented in Table 10. It can be seen that for a constant internal length μ, with increasing thickness, the frequency decreases as expected and the effect of increasing the internal length for a constant δ is to decrease the frequency. The combined effect of increasing the internal length and radius-to-thickness ratio is to decrease the frequency. The advantage of using NURBS is that the geometry is exactly represented and higher order continuous functions can be obtained with less computational effort.

Table 8 Control points and corresponding weights for a circular plate with radius R=0.5.

	1	2	3	4	5	6	7	8	9
x_i	$-\frac{\sqrt{2}}{4}$	$-\frac{\sqrt{2}}{2}$	$\frac{\sqrt{2}}{4}$	0	0	0	$\frac{\sqrt{2}}{4}$	$\frac{\sqrt{2}}{2}$	$\frac{\sqrt{2}}{4}$
y_i	$\frac{\sqrt{2}}{4}$	0	$-\frac{\sqrt{2}}{4}$	$\frac{\sqrt{2}}{2}$	0	$-\frac{\sqrt{2}}{2}$	$\frac{\sqrt{2}}{4}$	0	$-\frac{\sqrt{2}}{4}$
w_i	1	$\frac{\sqrt{2}}{2}$	1	$\frac{\sqrt{2}}{2}$	1	$\frac{\sqrt{2}}{2}$	1	$\frac{\sqrt{2}}{2}$	1

Table 9 Convergence of the non-dimensionalized fundamental frequencies for a clamped circular plate with μ=0.

Method	Order	Number of control points	Non-dimensionalized frequency (μ=0)		
			Ω_1	Ω_2	Ω_3
Ref. [71]	–	–	9.2751	17.8285	27.1041
IGA	Quadratic	7	9.3035	17.9918	27.3737
		9	9.2848	17.8804	27.1861
		11	9.2793	17.8500	27.1372
		13	9.2772	17.8390	27.1199
		15	9.2763	17.8342	27.1126
IGA	Cubic	7	9.2755	17.8346	27.1232
		9	9.2752	17.8295	27.1069
		11	9.2751	17.8287	27.1046
		13	9.2751	17.8285	27.1041
		15	9.2751	17.8284	27.1039

5 Conclusions

In this paper, after discussing two types of different nonlocal elasticity theories, the constitutive stress gradient proposed by Eringen was used to discuss Euler-Bernoulli nanobeams, Timoshenko beams and nanoplates based on Reissner-Mindlin formulation. The natural frequencies of the nanobeams and nanoplates are studied by employing Lagrange polynomials, MLS approximants and NURBS. Numerical experiments have been conducted to reveal the effect of boundary conditions and the nonlocal parameter on the natural frequencies of nanobeams and nanoplates. The results obtained by employing different basis functions are found to be in excellent agreement with the analytical results available in the literature. From the numerical studies, it can be seen that the NURBS basis functions require fewer degrees of freedom to yield the same order of accuracy as that of the radial basis functions in the case of beams. It can also be inferred that the effect of the nonlocal parameter is to reduce the natural frequency of nanoplates irrespective of the boundary conditions.

Table 10 Influence of the internal length on the non-dimensionalized fundamental frequency for a clamped circular plate. The influence of the thickness-to-radius ratio is also shown.

μ	$\delta=h/R$		
	0.1	0.15	0.2
0	9.9782	9.6648	9.2751
1	1.8381	1.7828	1.7146
2	1.3105	1.2710	1.2223
3	1.0730	1.0407	1.0008
4	0.9305	0.9025	0.8679
5	0.8330	0.8079	0.7769

References

[1] Born M, Huang K. *Dynamical Theory of Crystal Lattices*. Oxford University Press: Oxford, 1954.
[2] Maranganti R, Sharma P. *Phys. Rev. Lett*. 2007, 98, 195504–195507.
[3] Aifantis EC. *J. Eng. Mater. Technol*. 1984, 106, 326–330.
[4] Mindlin RD. *Arch. Rational Mech. Anal*. 1964, 16, 51–78.
[5] Mindlin RD, Tiersten HF. *Arch. Rational Mech. Anal*. 1962, 11, 415–448.
[6] Topin RA. *Arch. Rational Mech. Anal*. 1962, 11, 385–414.
[7] Koiter WT. *Proc. K. Ned. Akad. Wet. B* 1963, 67, 17–44.
[8] Yang F, Chong ACM, Lam DCC, Tong P. *Int. J. Solids Struct.* 2002, 39, 2731–2743.
[9] Ma HM,Gao X-L, Reddy JN. *J. Mech. Phys. Solids* 2008, 56, 3379–3391.
[10] Eringen AC. *J. Appl. Phys*. 1983, 54, 4703–4710.
[11] Eringen AC. *Int. J. Eng. Sci*. 1972, 10, 425–435.
[12] Eringen AC, Edelen DG. *Int. J. Eng. Sci*. 1972, 10, 233–248.
[13] Chen Y, Lee JD. *Int. J. Eng. Sci*. 2003, 41, 871–886.
[14] Peerlings RH, Fleck NA. *Int. J. Multiscale Comput. Eng*. 2004, 2, 599–619.
[15] Maranganti R, Sharma P. *J. Mech. Phys. Solids* 2007, 55, 1823–1852.
[16] Sun CT, Zhang H. *J. Appl. Phys*. 2003, 93, 1212.
[17] Reddy JN. *Int. J. Eng. Sci*. 2007, 45, 288–307.
[18] Aydogu M. *Physica* 2009, 41, 1651–1655.
[19] Phadikar JK, Pradhan SC. *Comput. Mater. Sci*. 2010, 49, 492–499.
[20] Wang Q. *J. Appl. Phys*. 2005, 98, 124301.
[21] Wang Q, Liew KM. *Phys. Lett. A* 2007, 363, 236–242.
[22] Wang Q, Varadan VK. *Smart Mater. Struct*. 2006, 15, 659–666.
[23] Ece MC, Aydogdu M. *Acta Mech*. 2007, 190, 185–195.
[24] Lu P, Lee HP, Lu C, Zhang PQ. *Int. J. Solids Struct.* 2007, 44, 5289–5300.
[25] Wang Q, Varadan VK, Quek ST. *Phys. Lett. A* 2006, 357, 130–135.
[26] Adalie S. *Phys. Lett. A* 2008, 372, 5701–5705.
[27] Zhang YQ, Liu GR, Wang JS. *Phys. Rev. B* 2004, 70, 205430–205435.
[28] Sudak LJ. *J. Appl. Phys*. 2003, 94, 7281.
[29] Duan WH, Wang CM. *Nanotechnology* 2007, 18, 385704.
[30] Duan WH, Wang CM, Zhang YY. *J. Appl. Phys*. 2007, 101, 024305.
[31] Lu P, Lee HP, Lu C, Zhang PQ. *J. Appl. Phys*. 2006, 99, 073510.
[32] Reddy JN, Pang SD. *J. Appl. Phys*. 2008, 103, 023511.
[33] Reddy JN. *Int. J. Eng. Sci*. 2010, 48, 1507–1518.
[34] Roque CMC, Ferreira AJM, Reddy JN. *Int. J. Eng. Sci*. 2011, 49, 976–984.
[35] Civalek O, Demir C. *Appl. Math. Model*. 2011, 35, 2053–2067.
[36] Murmu T, Pradhan SC. *Physica E* 2009, 41, 1628–1633.
[37] Ansari R, Rajabiehfard R, Arash B. *Comput. Mater. Sci*. 2010, 49, 831–838.
[38] Malekzadeh P, Setoodeh AR, Beni AA. *Compos. Struct*. 2011, 93, 1631–1639.
[39] Aghababaei R, Reddy JN. *J. Sound. Vib*. 2009, 326, 277–289.
[40] Ansari R, Sahmani S, Arash B. *Phys. Lett. A* 2010, 375, 53–62.
[41] Murmu T, Pradhan SC. *Mech. Res. Commun*. 2009, 36, 933–938.
[42] Murmu T, Pradhan SC. *Physica E* 2009, 41, 1232–1239.
[43] Pradhan SC. *Phys. Lett. A* 2009, 373, 4182–4188.
[44] Pradhan SC, Murmu T. *Comput. Mater. Sci*. 2009, 47, 268–274.
[45] Danesh M, Farajpour A, Mohammadi M. *Mech. Res. Commun*. 2012, 39, 23–27.
[46] Chandrasekar K, Mukherje S, Yu X. *Int. J. Solids Struct*. 2006, 43, 7128–7144.
[47] Ericksen JL. *Math. Mech. Solids* 2008, 13, 199–220.
[48] Pozrikidis C. *Comput. Mater. Sci*. 2009, 46, 438–442.
[49] Aifantis EC. *Int. J. Eng. Sci*. 1992, 30, 1279–1299.
[50] Ru CQ, Aifantis EC. *Acta Mech*. 1993, 101, 59–68.
[51] Gutkin MY, Aifantis EC. *Scripta Mater*. 1996, 35, 1353–1358.
[52] Altan BS, Aifantis EC. *J. Mech. Behavior Mater*. 1997, 8, 231–282.
[53] Gutkin MY, Aifantis EC. *Phys. Solid State* 1999, 41, 1980–1988.
[54] Askes H, Aifantis EC. *Int. J. Fracture* 2002, 117, 347–358.
[55] Teneketzis Tenek L, Aifantis EC. *Comput. Model. Eng. Sci.* 2002, 3, 731–741.
[56] Lazar M, Maugin GA, Aifantis EC. *Phys. Status Solidi B* 2005, 242, 2365–2390.
[57] Steinmann P, Ricker S, Aifantis E. *Arch. Appl. Mech*. 2011, 81, 669–684.
[58] Askes H, Aifantis EC. *Int. J. Solids Struct*. 2011, 48, 1962–1990.
[59] Aifantis EC. *Int. J. Eng. Sci*. 2011, 49, 1357–1367.
[60] Lazopoulos KA, Alnefaie KA, Abu-Hamdeh NH, Aifantis EC. The GRADELA plates & shells. In: *Proc. 10th Jubilee Int. Conf. on Shell Structures, Theory and Applications (SSTA 2013),* 16–18 October 2013, Gdansk/Poland, CRC Press/Balkema, 2013, pp. 121–124.
[61] Xu KY, Alnefaie KA, Abu-Hamdeh NH, Almitani KH, Aifantis EC. *Acta Mech. Solida Sinica*, 2014, 27, 345–352.
[62] Dasgupta S, Sengupta D. *Int. J. Numer. Meth. Eng*. 1990, 30, 419–430.
[63] Papaconstantopoulos SA, Zervos A, Vardoulakis I. *Int. J. Numer. Meth. Eng*. 2009, 77, 1396–1415.
[64] Hughes TJR, Cottrell JA, Bazilevs Y. *Comput. Meth. Appl. Mech. Eng*. 2005, 194, 4135–4195.
[65] Piegl L, Tiller W. *The NURBS Book*. Springer-Verlag: New York, 1997.
[66] Somashekar BR, Prathap G, Babu CR. *Comput. Struct*. 1987, 25, 345–353.
[67] Ganapathi M, Varadan TK, Sarma BS. *Comput. Struct*. 2011, 47, 325–334.
[68] Belytschko T, Gracie R, Ventura G. *Model. Simulat. Mater. Sci*. 2009, 17, 1–24.
[69] Hsu J-C, Lee H-L, Chang W-J. *Current Appl. Phys*. 2011, 11, 1384–1388.
[70] Singh KV. *Mech. Syst. Signal Process*. 2009, 23, 1870–1883.
[71] Hashemi SH, Bedroud M, Nazemnezhad R. *Compos. Struct.* 2013, 103, 108–118.